Spin-orbit-interaction activated interchannel coupling in dipole and quadrupole photoionization

S. Sunil Kumar,[1] T. Banerjee,[2] P. C. Deshmukh,[1,*] and S. T. Manson[3]
[1]*Department of Physics, Indian Institute of Technology Madras, Chennai 600036, India*
[2]*Manipal Institute of Technology, Manipal 576104, India*
[3]*Department of Physics and Astronomy, Georgia State University, Atlanta, Georgia 30303, USA*
(Received 16 January 2009; published 1 April 2009)

The effect of spin-orbit interaction activated interchannel coupling in dipole and quadrupole photoionization of the $4p$ and $4d$ subshells of Xe and the $5p$ and $5d$ subshells of Rn using the relativistic random phase approximation (RRPA) is studied. Interference between channels arising from spin-orbit split components is found to influence the dipole cross sections of Xe $4d$ and Rn $5d$ subshells, and also the quadrupole cross sections of Xe $4p$ and Rn $5p$ subshells. The photoelectron angular distribution parameters are also affected, but to a lesser extent. Using the understanding gained, the conditions required for large spin-orbit interaction activated interchannel coupling effects are delineated.

DOI: 10.1103/PhysRevA.79.043401 PACS number(s): 32.80.Fb, 32.10.Fn

I. INTRODUCTION

Interchannel coupling, i.e., correlation among the final continuum states of an ionizing transition, has been found to be of great importance for the understanding of the atomic photoionization process [1–4]. In particular, it has been found that the coupling of channels arising from spin-orbit split subshells can cause significant changes in the energy dependence of the photoionization parameters in the near-threshold region [5,6]. This effect is known as *spin-orbit interaction activated interchannel coupling* (SOIAIC). Interchannel coupling is known to affect weak photoionization channels that are degenerate with strong channels, especially near the ionization threshold [7]. Thus, the effect shows up in spin-orbit doublets in the situation where the cross section for the $j=l+1/2$ state is much smaller than the cross section for the $j=l-1/2$, in the region of the $j=l-1/2$ threshold. It was first identified [5] in an analysis of an experimental investigation of partial cross sections and angular distribution asymmetry parameters of the Xe $3d$ spin-orbit components [8]. Similar effects in the $3d$ subshell photoionization of Cs and Ba have been seen experimentally [9,10]. Furthermore, it has been shown that the effect of spin-orbit interaction activated interchannel coupling is also exhibited in quadrupole spin-polarization parameters and generalized oscillator strengths of $3d$ subshells of Xe, Cs, and Ba [11,12], and the SOIAIC effect has been found to influence dipole photoionization of Xe $3p$ [13], Xe $4d$ [14], and Hg $3d$ [15] as well. It is therefore of some interest to explore this phenomenon somewhat further.

In the present work, we have carried out calculations on dipole and quadrupole photoionization of the $4d$ and $4p$ subshells of Xe, and of the $5d$ and $5p$ subshells of Rn, in an effort to understand better where SOIAIC is important and why. Xe and Rn atoms were chosen for the present study as both are closed-shell atoms, and hence amenable to the relativistic random phase approximation (RRPA) methodology [16,17] employed in the present work. The $4d$ and the $4p$ subshells of Xe, and the $5d$ and the $5p$ subshells of Rn, offer themselves as interesting subjects for the interchannel coupling effects investigated in the present work due to their spin-orbit splitting, and also due to the fact that the centrifugal barrier faced by the continuum wave functions involved in the corresponding dipole/quadrupole photoionization channels which plays a significant role in the manifestation of the SOIAIC effect.

II. BRIEF THEORETICAL DETAILS

The RRPA methodology is based upon the Dirac equation, and hence relativistic effects, including the spin-orbit splittings of the atomic subshells, are included explicitly. The method is thus admirably suited for application to SOIAIC study. In addition, RRPA includes significant aspects of multielectron correlation effects, including initial-state correlation and interchannel coupling. The RRPA builds in electron correlations starting with a Dirac-Fock initial state and includes all "two-electron-two-hole" Coulomb direct and exchange-correlation diagrams. The inclusion of time-backward diagrams enables one to include many of the important correlations in the initial state of the photoionization process, while the inclusion of the time-forward diagrams enables one to address correlations resulting from interchannel coupling in the final state. The details of the RRPA methodology are discussed in detail elsewhere [16,17].

Another useful feature of the RRPA methodology is that the number of interacting photoionization channels can be varied, i.e., the RRPA can be truncated. Of course, the calculation including coupling among all of the relativistic single-excitation channels arising from the photoionization of the ground state of the atom is the most accurate. But, truncation provides insight into the effects of a specific coupling on the result; thus our calculations for each case have been performed at two different levels of truncation, as follows:

For dipole photoionization from the np subshell

Level 1: $np_{1/2} \rightarrow s, d_{3/2}$(two channels);

$np_{3/2} \rightarrow s, d_{3/2}, d_{5/2}$(three channels);

*pcd@physics.iitm.ac.in

 ©2009 The American Physical Society

Level 2: $np_{1/2} \rightarrow s, d_{3/2}$;

$np_{3/2} \rightarrow s, d_{3/2}, d_{5/2}$(five channels).

For dipole photoionization from the *nd* subshell,

Level 1: $nd_{3/2} \rightarrow p_{1/2}, p_{3/2}, f_{5/2}$(three channels);

$nd_{5/2} \rightarrow p_{3/2}, f_{5/2}, f_{7/2}$(three channels),

Level 2: $nd_{3/2} \rightarrow p_{1/2}, p_{3/2}, f_{5/2}$;

$nd_{5/2} \rightarrow p_{3/2}, f_{5/2}, f_{7/2}$(six channels).

For quadrupole photoionization from the *np* subshell

Level 1: $np_{1/2} \rightarrow p_{3/2}, f_{5/2}$(two channels);

$np_{3/2} \rightarrow p_{1/2}, p_{3/2}, f_{5/2}, f_{7/2}$(four channels),

Level 2: $np_{1/2} \rightarrow p_{3/2}, f_{5/2}$;

$np_{3/2} \rightarrow p_{1/2}, p_{3/2}, f_{5/2}, f_{7/2}$(six channels).

For quadrupole photoionization from the *nd* subshell,

Level 1: $nd_{3/2} \rightarrow s, d_{3/2}, d_{5/2}, g_{7/2}$(four channels);

$nd_{5/2} \rightarrow s, d_{3/2}, d_{5/2}, g_{7/2}, g_{9/2}$(five channels),

Level 2: $nd_{3/2} \rightarrow s, d_{3/2}, d_{5/2}, g_{7/2}$;

$nd_{5/2} \rightarrow s, d_{3/2}, d_{5/2}, g_{7/2}, g_{9/2}$(nine channels).

Computations at Level 1 will be referred to as *pseudoindependent particle truncation* (PIPT) since they include only coupling among the channels arising from a given nl_j subshell. The Level 2 calculations will be referred to as *intrasubshell truncation* (ISST) since they include also the interchannel coupling between the nl_j spin-orbit doublet photoionization channels, $j=l+1/2$ and $j=l-1/2$. It is to be emphasized that a full calculation, which includes interchannel coupling with the photoionization channels arising from all of the other $n'l'_{j'}$ subshells, has not been performed. Although the full nontruncated calculation would evidently be closest to experiment, the purpose of this work is to highlight the effects of the interchannel coupling among the spin-orbit doublets. Furthermore, the omitted channels have only a minor effect in the energy ranges considered herein.

Note that when all possible single-particle excitations/ionizations are included in the RRPA calculation, the full nontruncated calculation, cross sections calculated in the "length" and "velocity" [17] formulations are identically equal [16,17]. But, for truncated RRPA calculations, this is not strictly true. For the results presented in this paper, however, "length" and "velocity" results generally agree to within about 5%. Thus, in this paper we ignore the differences and present only results in the length formulation.

Since experimental binding energies are available for atomic Xe [18], we have replaced the Dirac-Fock (DF) thresholds by the experimental thresholds while performing the RRPA calculations for Xe. In the case of atomic Rn, however, experimental data are scanty and hence DF thresholds were employed. The thresholds of the subshells for which photoionization is reported in this work are given in Table I.

TABLE I. The thresholds of the subshells for which photoionization is reported in the present work.

Subshell	DF threshold (eV)	Expt. threshold (eV) [18]
Xe $4d_{5/2}$	71.669	67.6
Xe $4d_{3/2}$	73.780	69.5
Xe $4p_{3/2}$	162.802	156.5
Xe $4p_{1/2}$	175.583	163.9
Rn $5d_{5/2}$	54.875	
Rn $5d_{3/2}$	59.586	
Rn $5p_{3/2}$	140.845	
Rn $5p_{1/2}$	174.400	

III. RESULTS AND DISCUSSION

A. Dipole photoionization

The partial cross sections for Xe $4d_{5/2}$ and $4d_{3/2}$ at the two levels of truncation described above are shown in Fig. 1 where it is seen that, at the quasiindependent particle (PIPT) level, both cross sections exhibit a substantial shape resonance of about 25 Mb. Furthermore, the maxima are seen to occur at roughly the same energy. This is very different from the inner-shell $3d$ cases in Xe, Cs, and Ba studied earlier [5,6,8–10] which also exhibit similar shape resonances but where the $j=5/2$ cross section is quite a bit smaller than the $j=3/2$ in the vicinity of the $j=3/2$ shape resonance. This difference is a consequence of the fact that the $3d$ thresholds

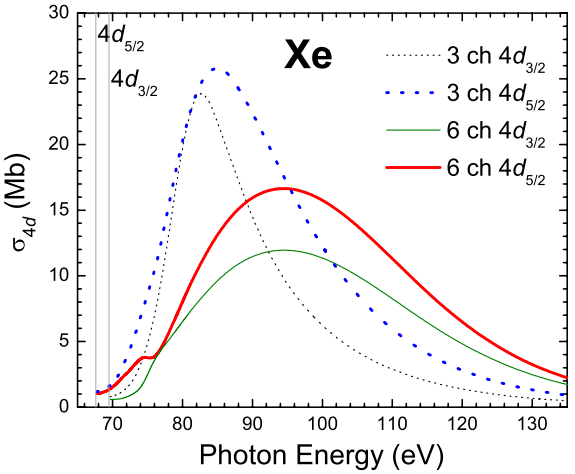

FIG. 1. (Color online) Xe $4d$ partial cross sections in the dipole approximation. Results are shown in the PIPT and ISST levels of truncation of the RRPA. The vertical lines indicate the threshold energies.

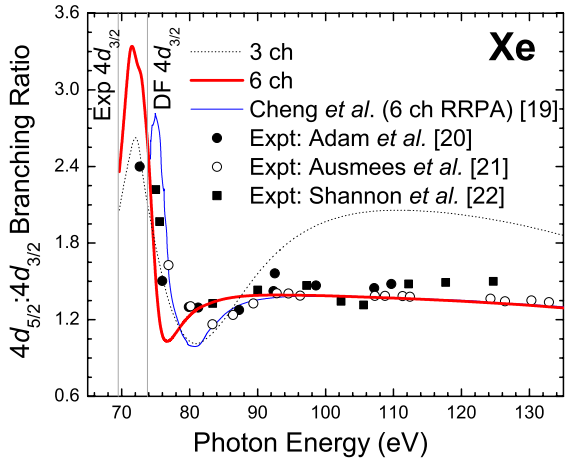

FIG. 2. (Color online) Xe $4d$ dipole branching ratio ($4d_{5/2}$:$4d_{3/2}$). The present three channel (dotted) and six channel (thick solid) are compared with earlier theoretical [19] (thin solid) and experimental [20] (solid circles) [21], (open circles) and [22] (solid squares) results. The vertical lines indicate the experimental and Dirac-Fock (DF) $4d_{3/2}$ thresholds.

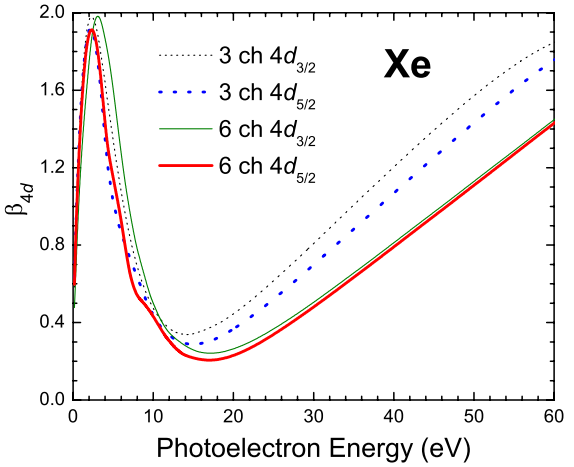

FIG. 3. (Color online) Dipole angular distribution asymmetry parameter β for Xe $4d$ as a function of photoelectron energy. Results are shown in the PIPT and ISST levels of truncation of the RRPA.

are separated by ~15 eV, but the $4d$ thresholds only by about 2 eV, as seen in Fig. 1. This difference suggests that the manifestations of interchannel coupling are likely to be different in the $3d$ and $4d$ cases. The results of the coupled (ISST) calculation, seen in Fig. 1, indicate that both $4d$ cross sections are affected strongly by interchannel coupling; both shape resonances become broader and lower, and the $4d_{5/2}$ cross section acquires a low-energy kink. It is evident that the kink in the ISST result for the $4d_{5/2}$ cross section at about 5 eV above the ionization threshold is absent in the PIPT calculation. Therefore, this structure in the $4d_{5/2}$ cross section must be a result of interchannel coupling with the $4d_{3/2}$ photoionization channels, i.e., the SOIAIC effect. For the $3d$ case, instead of a kink, a dip and second maximum are found; this is a consequence of the difference in the spin-orbit split thresholds in the two cases. In addition, it was seen that, for Xe $3d$ photoionization [5,6], a major effect of interchannel coupling was to alter the $3d_{5/2}$ cross section in the vicinity of the $3d_{3/2}$ shape resonance; as a general rule, the dominant effect of interchannel coupling is the alteration of the smaller of the degenerate cross sections [7]. For Xe $4d$ photoionization neither cross section is much larger than the other, and the phenomenology is seen to be rather different. This point shall be addressed in detail below.

Though the kink in the cross section of Xe $4d_{5/2}$ is rather small, the effect is well identified in the branching ratio of the cross sections, as can be seen from Fig. 2, where the earlier RRPA result [19] is also shown along with various experimental results [20–22]. The small disagreement between the present RRPA result and that of Ref. [19] is partially due to the fact that experimental thresholds [18] have been employed in the present work, whereas the Dirac-Fock thresholds were employed in [19]. It is to be noted that all theoretical and experimental results deviate significantly from the statistical ratio (1.5) up to about 20 eV above the ionization thresholds. The departure of the branching ratio from the statistical ratio is clearly due to spin-orbit interaction activated interchannel coupling.

Even though the interchannel coupling changes the $4d_j$ cross sections significantly, this significant alteration is not reflected in the angular distribution asymmetry parameter β, as seen in Fig. 3. This is because β is given by a ratio of matrix elements, and the effects of interchannel coupling largely wash out in the ratio, even though they are significant in both numerator and denominator. Thus, as a general rule, β may not be a very good indicator of interchannel coupling effects, spin-orbit interaction activated or otherwise.

In order to gain further insight into the SOIAIC effect, the absolute values of the photoionization matrix elements for the uncoupled, PIPT, calculation and the coupled, ISST, calculation in Figs. 4 and 5 respectively, are shown; absolute values are shown since correlation renders the dipole matrix elements complex. From Fig. 4 it is seen that the three $4d \rightarrow f$ matrix elements dominate the photoionization process (except right at the thresholds) and, of the three, the $4d_{5/2} \rightarrow f_{5/2}$ is much smaller than the other two. Thus, one expects

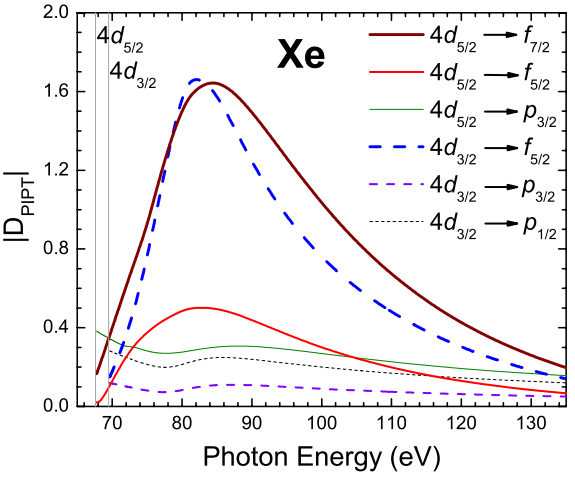

FIG. 4. (Color online) Absolute values of dipole matrix elements for Xe $4d$ when channels from $4d_{3/2}$ and $4d_{5/2}$ *are not coupled* (PIPT). The vertical lines indicate the threshold energies.

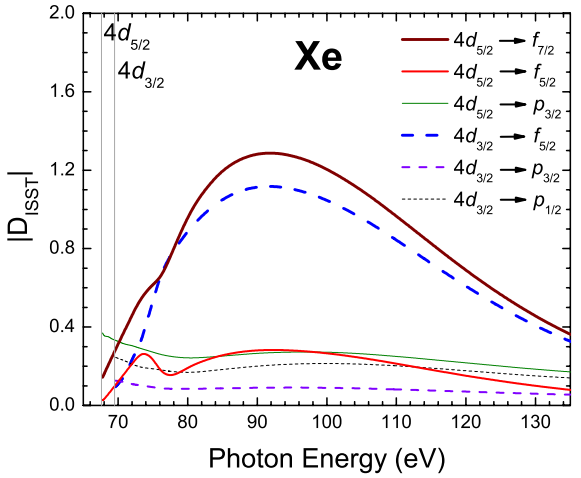

FIG. 5. (Color online) Absolute values of dipole matrix elements for Xe $4d$ when channels from $4d_{3/2}$ and $4d_{5/2}$ *are coupled* (ISST). The vertical lines indicate the threshold energies.

the interchannel coupling to affect this smaller amplitude most strongly. This is, in fact, the case, as seen in Fig. 5 which demonstrates that the kink is almost entirely due to the effect of interchannel coupling upon this smaller amplitude. An effect on the $4d_{5/2} \rightarrow f_{7/2}$ is also seen, but the effect is much smaller since this $4d_{5/2} \rightarrow f_{7/2}$ amplitude is much larger than $4d_{5/2} \rightarrow f_{5/2}$. In addition, an overall broadening and flattening of the $4d \rightarrow f$ amplitudes is seen in Fig. 5, with the smallest amplitude, $4d_{5/2} \rightarrow f_{5/2}$, experiencing the largest change.

Similar truncated RRPA calculations have been performed for dipole photoionization of Rn $5d$; the cross sections for both levels of truncation are shown in Fig. 6 for the $j=5/2$ and 3/2 subshells. The results are seen to be similar to the Xe $4d$ case. The cross sections are broadened and lowered by the interchannel coupling, and the $j=5/2$ cross section again acquires a kink, a significantly more prominent kink than in the Xe $4d$ case, however. Evidently the interchannel coupling effects are stronger for the Rn $5d$ subshells. The increase in interchannel effects is due primarily to the increased spin-orbit splitting in this case as opposed to the Xe $4d$ case, along with the increase in other relativistic effects. This kink translates to a strong dip in the branching ratio (not shown); this branching ratio has not yet been looked at experimentally, but the present results suggest that such a study would prove most interesting.

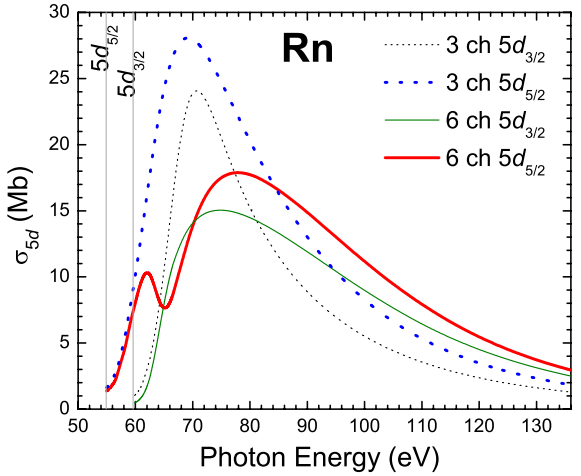

FIG. 6. (Color online) Rn $5d$ partial cross sections in the dipole approximation. Results are shown in the PIPT and ISST levels of truncation of the RRPA. The vertical lines indicate the threshold energies.

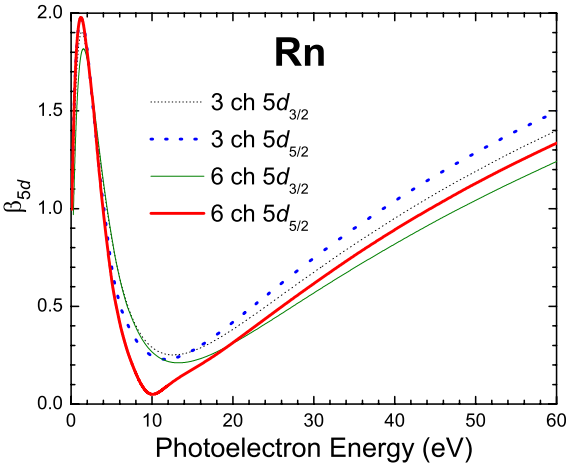

FIG. 7. (Color online) Dipole angular distribution asymmetry parameter β for Rn $5d$ as a function of photoelectron energy. Results are shown in the PIPT and ISST levels of truncation of the RRPA.

Results for the photoelectron angular distribution asymmetry parameter β, shown in Fig. 7, are very similar to the Xe case, with one exception; in the neighborhood of the kink in the $5d_{5/2}$ cross section, which was seen to occur about 10 eV above threshold, the six-channel $5d_{5/2}$ β shows a decided dip reflecting the kink.

Absolute values of the matrix elements of Rn $5d$ photoionization are shown in Fig. 8 (PIPT) and Fig. 9 (ISST). The matrix elements corresponding to the transitions $5d_{5/2} \rightarrow f_{7/2}$, $5d_{5/2} \rightarrow f_{5/2}$, and $5d_{3/2} \rightarrow f_{5/2}$ exhibit shape resonances. The

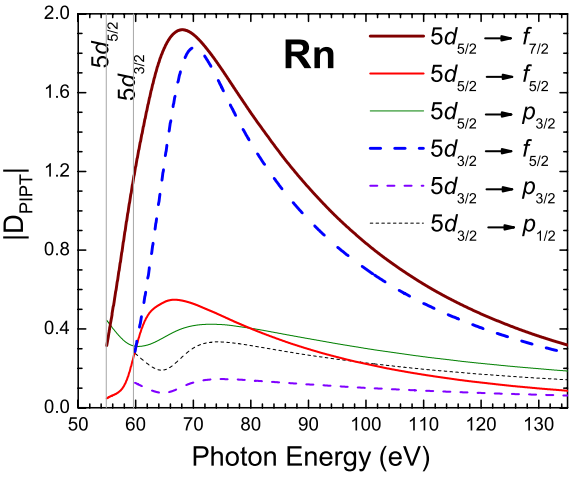

FIG. 8. (Color online) Absolute values of dipole matrix elements for Rn $5d$ when channels from $5d_{3/2}$ and $5d_{5/2}$ *are not coupled* (PIPT). The vertical lines indicate the threshold energies.

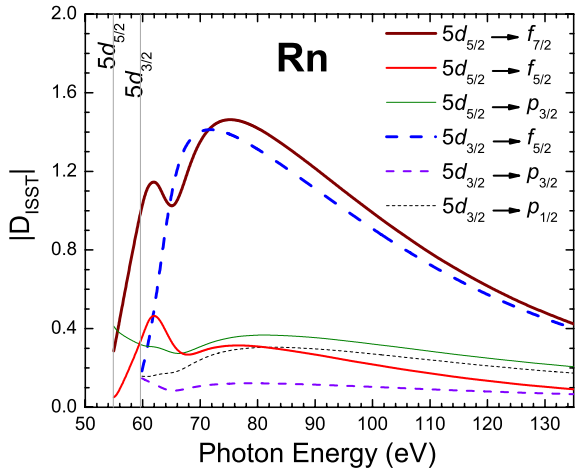

FIG. 9. (Color online) Absolute values of dipole matrix elements for Rn $5d$ when channels from $5d_{3/2}$ and $5d_{5/2}$ *are coupled* (ISST). The vertical lines indicate the threshold energies.

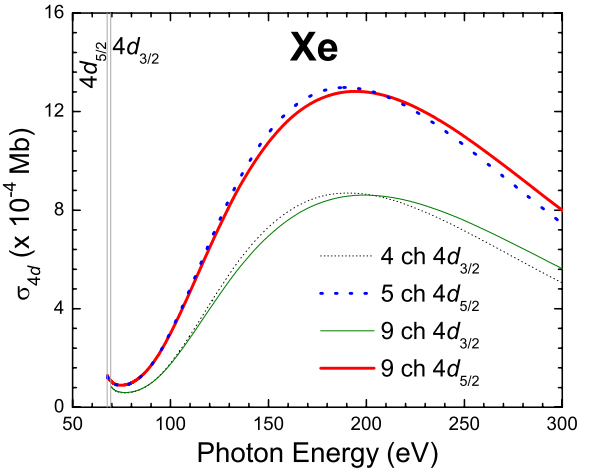

FIG. 10. (Color online) Xe $4d$ partial cross sections in the quadrupole approximation. Results are shown in the PIPT and ISST levels of truncation of the RRPA. The vertical lines indicate the threshold energies.

photoionization channels from the $5d_{3/2}$ subshell open at a slightly higher energy than $5d_{5/2}$, and strong interchannel coupling effects are seen in Fig. 9 primarily due to interference among $5d_{5/2} \rightarrow f_{5/2}$, $5d_{3/2} \rightarrow f_{5/2}$, and $5d_{5/2} \rightarrow f_{7/2}$ channels, resulting in the significant dip in the $5d_{5/2} \rightarrow f_{5/2}$, and $5d_{5/2} \rightarrow f_{7/2}$ matrix elements at $h\nu \sim 65$ eV. As in the case of Xe $4d$, this interference manifests only in the six-channel ISST case (Fig. 9) but not in the case of PIPT (Fig. 8), so it must be due to the coupling between the $5d_{5/2}$ and $5d_{3/2}$ photoionization channels, i.e., the structure is clearly due to the SOIAIC effect. Here also, in addition to generating the structure in the $5d_{5/2} \rightarrow f_{5/2}$, and $5d_{5/2} \rightarrow f_{7/2}$ matrix elements, complex mixing among the strong matrix elements modifies the cross section over almost the entire energy range.

Calculations of the dipole photoionization of Xe $4p$ and Rn $5p$ (not shown) do not exhibit any significant effect of SOIAIC. Evidently, this is because of the fact that the cross sections of the $j=l+1/2$ channels are not small compared to the cross sections of the $j=l-1/2$ channels, in these cases; centrifugal barrier effects which are large enough to produce significant delayed maxima are required, which appears to mean that continuum waves of $l=3$ are required, at least for Xe and Rn. However, quadrupole photoionization couples these np states to the f-wave continuum so that SOIAIC effects might be expected in such cases; this is considered in Sec. III B.

B. Quadrupole photoionization

To test the inference concerning the possibility of quadrupole SOIAIC effects, and since there have been only a few studies on correlation effects in quadrupole photoionization [23–25], RRPA calculations have been carried out for the Xe $4d$, Rn $5d$, Xe $4p$, and Rn $5p$ subshells, using both PIPT and ISST levels of truncation, just as for the dipole photoionization case presented above.

RRPA results for the quadrupole photoionization cross sections for Xe $4d$ and Rn $5d$ subshells are shown, respectively, in Figs. 10 and 11 at both PIPT and ISST levels. Very little difference is seen between the results of these two levels of calculation, which means that interchannel coupling hardly influences the quadrupole photoionization cross section in these two cases. A strong delayed maximum in the quadrupole photoionization cross section due to the centrifugal barrier faced by the final εg states involved in the quadrupole transitions is exhibited, but it is so delayed that it does not contribute appreciably to the cross sections in the near-threshold region. This delayed maximum is preceded by a small dip in the cross section just above the threshold, both for Xe $4d$ and the Rn $5d$ cases. To understand this dip, in Fig. 12 the absolute values of the quadrupole matrix elements for Xe $4d$ are shown (only ISST results are shown as the PIPT results are almost the same, in this case). Here it is seen that while the $4d \rightarrow \varepsilon g$ quadrupole channels get stronger as the photon energy increases above the threshold, peaking toward the maximum of the corresponding shape resonance,

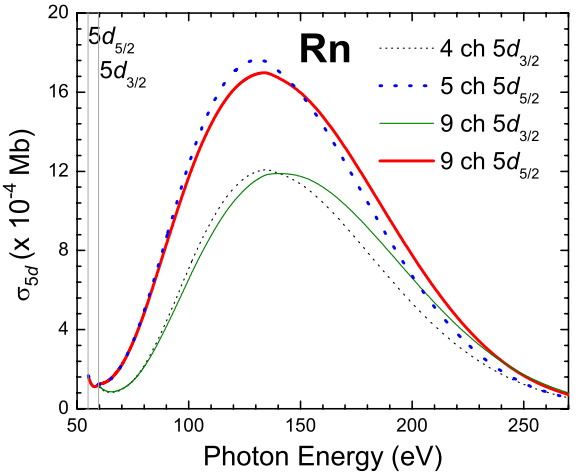

FIG. 11. (Color online) Rn $5d$ partial cross sections in the quadrupole approximation. Results are shown in the PIPT and ISST levels of truncation of the RRPA. The vertical lines indicate the threshold energies.

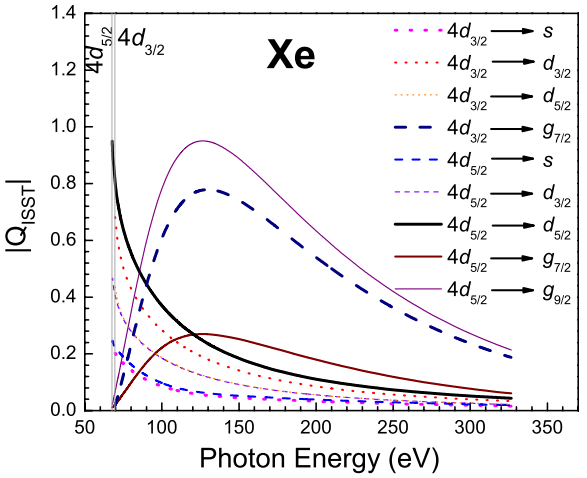

FIG. 12. (Color online) Absolute values of quadrupole matrix elements for Xe $4d$ when channels from $4d_{3/2}$ and $4d_{5/2}$ *are coupled* (ISST). The vertical lines indicate the threshold energies.

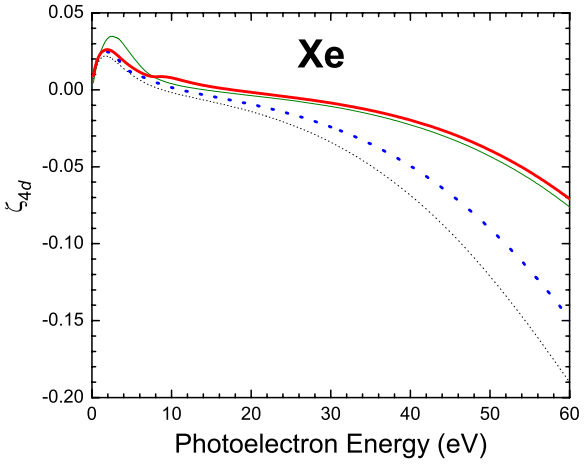

FIG. 13. (Color online) Nondipole angular distribution asymmetry parameter ζ for Xe $4d$ as a function of photoelectron energy. Thick and thin dotted curves are the uncoupled (PIPT) $4d_{5/2}$ and $4d_{3/2}$ ζ, respectively, and the corresponding solid curves are respective coupled (ISST) results.

the strength in the $4d \rightarrow \varepsilon d$ and $4d \rightarrow \varepsilon s$ channels decrease with energy. In the region of the crossover of these competing channels, the photoionization cross section, which is determined by the sum of the squares of all of these matrix elements, shows a dip since the channels that are decreasing with energy dominate in the threshold region. No feature is seen in the quadrupole cross sections or the corresponding matrix elements that has in it any perceptible influence of the SOIAIC effect; the situation for Rn $5d$ is essentially the same.

While there is no SOIAIC effect on the quadrupole matrix elements (and cross sections), it is however noticed in the corresponding nondipole angular distribution asymmetry parameter ζ which is equal to $(\gamma+3\delta)$, γ and δ being given in [18]. This is due to the fact that the nondipole parameter ζ depends upon both the quadrupole amplitudes and the dipole amplitudes [18], the latter being affected by SOIAIC. This is seen from a comparison of the PIPT and ISST truncation level results of ζ, shown in Figs. 13 and 14, respectively, for Xe $4d$ and Rn $5d$ subshells. However, since the angular distribution parameter ζ, like β, is given by a ratio of matrix elements, the effect(s) of interchannel coupling are relatively small. Both Xe $4d$ and Rn $5d$ display some structure for small photoelectron energies. The coupled (ISST) results are almost exactly the same for Xe $4d_{5/2}$ and $4d_{3/2}$, indicating a cancellation of interchannel coupling effects, but for Rn $5d_{5/2}$ and $5d_{3/2}$, differences are seen; interchannel coupling effects do not quite cancel out here most likely due to the fact that the Rn $5d$ subshells are significantly more relativistic than Xe $4d$, and this results in dynamical differences between $5d_{5/2}$ and $5d_{3/2}$. Note, for example, the differences in near-threshold structure between Rn $5d_{5/2}$ and $5d_{3/2}$, seen in Fig. 14. In any case, it is evident from Figs. 13 and 14 that the nondipole parameters are small over the whole threshold region. Note further that the composite nondipole parameter $\zeta = \gamma+3\delta$, where γ and δ are the individual nondipole parameters [18]. ζ is presented, rather than γ and δ individually for two reasons: first, the dynamical effects are essentially the same in all three parameters, so it somewhat redundant to present γ and δ, and second, many experiments measure ζ rather than γ and/or δ [18] by themselves.

The calculated quadrupole photoionization cross sections for Xe $4p_{1/2}$ and $4p_{3/2}$ subshells are shown in Fig. 15 and the behavior is strikingly similar to that of dipole photoionization from the $3d$ subshell of Xe [5], and for pretty much the same reasons. The crucial ingredient for the significant manifestation of SOIAIC in the Xe $3d$ dipole case was seen to be the shape resonance in the εf continua, which are accessible to the $3d$ initial states via dipole transitions. In the quadrupole case, the $4p$ initial states can couple to the same continua via the absorption of quadrupole photons, thereby resulting in very similar phenomenology, as seen in Fig. 15.

The SOIAIC effect is not significant in the case of dipole photoionization of the Xe $4p$ subshell, as mentioned above, despite which the nondipole photoelectron angular distribu-

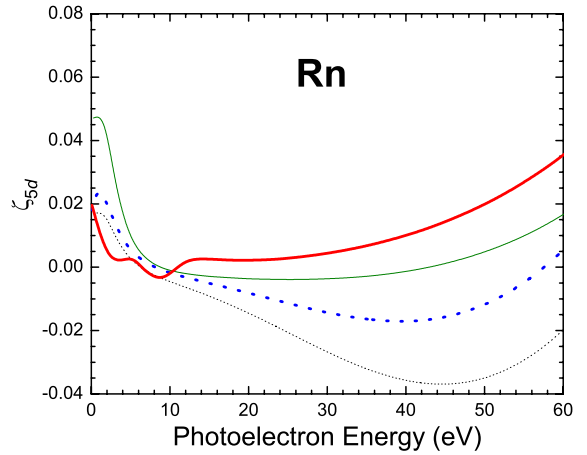

FIG. 14. (Color online) Nondipole angular distribution asymmetry parameter ζ for Rn $5d$ as a function of photoelectron energy. Thick and thin dotted curves are the uncoupled (PIPT) $5d_{5/2}$ and $5d_{3/2}$ ζ, respectively, and the corresponding solid curves are respective coupled (ISST) results.

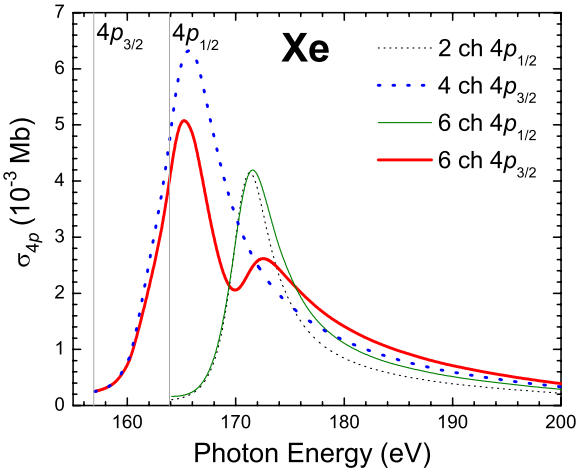

FIG. 15. (Color online) Xe $4p$ partial cross sections in the quadrupole approximation. Results are shown in the PIPT and ISST levels of truncation of the RRPA. The vertical lines indicate the threshold energies.

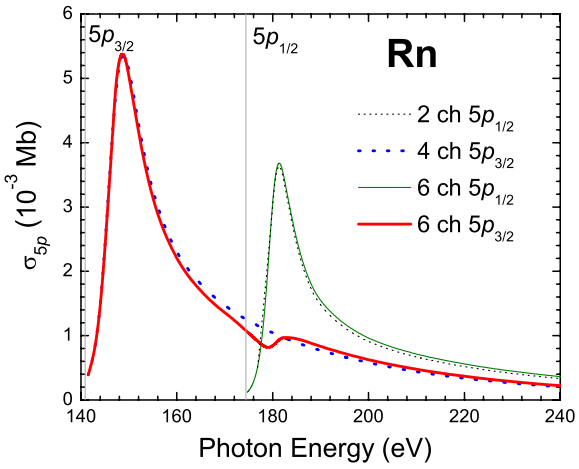

FIG. 17. (Color online) Rn $5p$ partial cross sections in the quadrupole approximation. Results are shown in the PIPT and ISST levels of truncation of the RRPA. The vertical lines indicate the threshold energies.

tion asymmetry parameter ζ for Xe $4p_{1/2}$ and $4p_{3/2}$ subshells, shown in Fig. 16, shows signs of SOIAIC effects. Since the parameter depends upon both dipole and quadrupole amplitudes [18], it is evident that the occurrence of SOIAIC effects in the quadrupole amplitudes is responsible for these the SOIAIC structure in the ζ parameters corresponding to Xe $4p$. For $4p_{3/2}$, the effects are seen to show up only in the vicinity of the kink in the $4p_{3/2}$ cross section, but for $4p_{1/2}$, interchannel coupling effects are in evidence over a larger energy range. In addition, the Xe $4p_j$ subshells show rather large dynamical differences between them since they are rather relativistic, i.e., the radial-wave functions in initial and final states are j dependent. Furthermore, the ζ parameter for $4p_{1/2}$ is rather large, reaching a value of about -0.5 approximately 8 eV above threshold. The $4p_{3/2}$ ζ, does not become nearly as large because of an accidental partial cancellation of individual terms in the sum for the calculation of ζ [18]; the accidental cancellation does not, however, occur for the $4p_{1/2}$ case.

The quadrupole photoionization cross section for Rn $5p_{1/2}$ and $5p_{3/2}$ is shown in Fig. 17. In this case, the atomic number being rather high, the spin-orbit splitting is so much that the quadrupole $5p_{3/2}$ photoionization cross section is already quite small, being well above the shape resonance peak, at the $5p_{1/2}$ photoionization threshold. Thus, in the neighborhood of the $5p_{1/2}$ shape resonance, the uncoupled $5p_{3/2}$ cross section is about a factor of 4 smaller than the $5p_{1/2}$. Despite this difference in cross section, interchannel coupling results in only a small effect on the $5p_{3/2}$ cross section, and almost none at all on the $5p_{1/2}$ result. This is because the splitting of the thresholds is so large, about 40 eV, that the interchannel coupling matrix element is quite small in the region of the $5p_{1/2}$ threshold, owing to the relatively poor overlap between the εf wave functions corresponding to $5p_{1/2}$ and $5p_{3/2}$

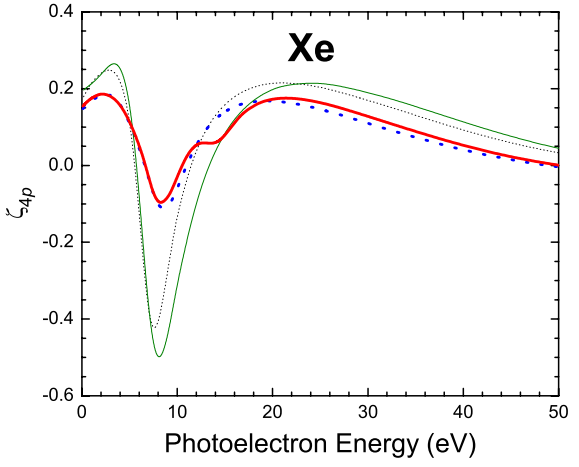

FIG. 16. (Color online) Nondipole angular distribution asymmetry parameter ζ for Xe $4p$ as a function of photoelectron energy. Thick and thin dotted curves are the uncoupled (PIPT) $4p_{3/2}$ and $4p_{1/2}$ ζ, respectively, and the corresponding solid curves are respective coupled (ISST) results.

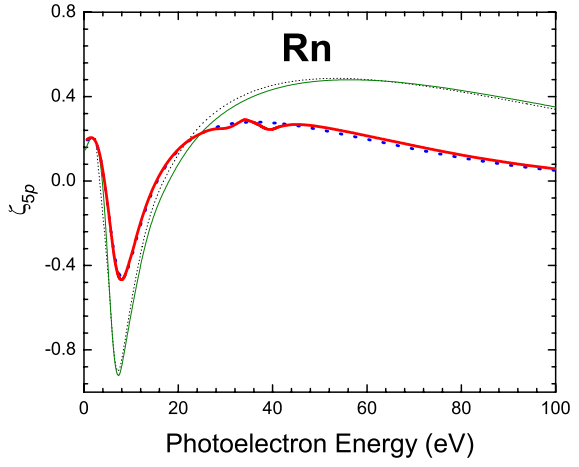

FIG. 18. (Color online) Nondipole angular distribution asymmetry parameter ζ for Rn $5p$ as a function of photoelectron energy. Thick and thin dotted curves are the uncoupled (PIPT) $5p_{3/2}$ and $5p_{1/2}$ ζ, respectively, and the corresponding solid curves are respective coupled (ISST) results.

photoionization, respectively. In other words, in the $5p_{1/2}$ threshold region, for the εf corresponding to $5p_{3/2}$ ionization, $\varepsilon \sim 40$ eV, while for the εf corresponding to $5p_{1/2}$, $\varepsilon \sim 0$ eV, resulting in a small overlap in the interchannel coupling matrix element. This indicates that SOIAIC becomes important only when the spin-orbit splitting of the nl_j subshells is relatively small.

The angular distribution asymmetry parameter ζ for photoionization of Rn $5p_{1/2}$ and $5p_{3/2}$, shown in Fig. 18, exhibits almost no SOIAIC effect, since neither the dipole nor quadrupole channels do. However, there is a rather large dynamical difference between the spin-orbit split channels, owing to relativistic effects. Furthermore, at the maxima in the quadrupole cross sections, rather large values of ζ are found, indicating that the quadrupole channels contribute significantly to the photoelectron angular distribution.

IV. CONCLUDING REMARKS

The influence of spin-orbit interaction activated interchannel coupling has been explored for four subshells of Xe and Rn in both dipole and quadrupole photoionization manifolds using the RRPA calculational methodology at several levels of truncation to spotlight the effect(s) of interchannel interactions. From these results, it is inferred that the conditions for SOIAIC to be important are the existence of a strong shape resonance near threshold, and relatively small spin-orbit splitting in the energies of the nl_j thresholds, but large enough so that the cross section of the $j=l+1/2$ subshell is smaller than the $j=l-1/2$ in the vicinity of the $j=l-1/2$ shape resonance. The effects are manifest in the subshell cross sections and branching ratios. They are less important in the photoelectron angular distribution parameters, dipole and nondipole, because these quantities are ratios of matrix elements and the interchannel effects tend to cancel out in the ratios.

ACKNOWLEDGMENTS

This work is partially supported by research grants from UGC, DST, NSF, and DOE, Division of Chemical Sciences.

[1] O. Hemmers, S. T. Manson, M. M. SantáAnna, P. Focke, H. Wang, I. A. Sellin, and D. W. Lindle, Phys. Rev. A **64**, 022507 (2001).
[2] P. C. Deshmukh, Radiat. Phys. Chem. **70**, 515 (2004).
[3] D. L. Hansen, O. Hemmers, H. Wang, D. W. Lindle, P. Focke, I. A. Sellin, C. Heske, H. S. Chakraborty, P. C. Deshmukh, and S. T. Manson, Phys. Rev. A **60**, R2641 (1999).
[4] E. W. B. Dias, H. S. Chakraborty, P. C. Deshmukh, S. T. Manson, O. Hemmers, P. Glans, D. L. Hansen, H. Wang, S. B. Whitfield, D. W. Lindle, R. Wehlitz, J. C. Levin, I. A. Sellin, and R. C. C. Perera, Phys. Rev. Lett. **78**, 4553 (1997).
[5] M. Ya. Amusia, L. V. Chernysheva, S. T. Manson, A. M. Msezane, and V. Radojević, Phys. Rev. Lett. **88**, 093002 (2002).
[6] V. Radojević, D. M. Davidović, and M. Ya. Amusia, Phys. Rev. A **67**, 022719 (2003).
[7] U. Fano and J. W. Cooper, Rev. Mod. Phys. **40**, 441 (1968).
[8] A. Kivimäki, U. Hergenhahn, B. Kempgens, R. Hentges, M. N. Piancastelli, K. Maier, A. Rüdel, J. J. Tulkki, and A. M. Bradshaw, Phys. Rev. A **63**, 012716 (2000).
[9] H. Farrokhpour, M. Alagia, M. Ya. Amusia, L. Avaldi, L. V. Chernysheva, M. Coreno, M. de Simone, R. Richter, S. Stranges, and M. Tabrizchi, J. Phys. B **39**, 765 (2006).
[10] T. Richter, E. Heinecke, P. Zimmermann, K. Godehusen, M. Yalçinkaya, D. Cubaynes, and M. Meyer, Phys. Rev. Lett. **98**, 143002 (2007).
[11] M. Ya. Amusia, N. A. Cherepkov, L. V. Chernysheva, Z. Felfli, and A. Z. Msezane, J. Phys. B **38**, 1133 (2005).
[12] M. Ya. Amusia, L. V. Chernysheva, Z. Felfli, and A. Z. Msezane, Phys. Rev. A **73**, 062716 (2006).
[13] P. C. Deshmukh, H. R. Varma, T. Banerjee, and S. T. Manson, Bull. Am. Phys. Soc. **48**, 41 (2003).
[14] K. P. Sunanda, T. Banerjee, H. R. Varma, U. Momeen, and P. C. Deshmukh, *XV National Conference on Atomic and Molecular Physics* (Physical Research Laboratory, Ahmedabad, India, 2004) p. 87.
[15] T. Banerjee, Ph. D. thesis, Indian Institute of Technology Madras, 2007.
[16] W. R. Johnson and C. D. Lin, Phys. Rev. A **20**, 964 (1979).
[17] A. F. Starace, in *Handbuch der Physik*, edited by W. Mehlhorn (Springer-Verlag, Berlin, 1982), Vol. 31, p. 23.
[18] A. Derevianko and W. R. Johnson, At. Data Nucl. Data Tables **73**, 153 (1999).
[19] K. T. Cheng and W. R. Johnson, Phys. Rev. A **28**, 2820 (1983).
[20] M. Y. Adam, F. Wuilleumier, S. Krummacher, N. Sandner, V. Schmidt, and W. Mehlhorn, J. Electron Spectrosc. Relat. Phenom. **15**, 211 (1979).
[21] A. Ausmees, S. J. Osborne, R. Moberg, S. Svensson, S. Aksela, O.-P. Sairanen, A. Kivimäki, A. Naves de Brito, E. Nõmmiste, J. Jauhiainen, and H. Aksela, Phys. Rev. A **51**, 855 (1995).
[22] S. P. Shannon, K. Codling, and J. B. West, J. Phys. B **10**, 825 (1977).
[23] O. Hemmers, R. Guillemin, E. P. Kanter, B. Krässig, D. W. Lindle, S. H. Southworth, R. Wehlitz, J. Baker, A. Hudson, M. Lotrakul, D. Rolles, W. C. Stolte, I. C. Tran, A. Wolska, S. W. Yu, M. Ya. Amusia, K. T. Cheng, L. V. Chernysheva, W. R. Johnson, and S. T. Manson, Phys. Rev. Lett. **91**, 053002 (2003).
[24] T. Banerjee, P. C. Deshmukh, and S. T. Manson, Phys. Rev. A **75**, 042701 (2007).
[25] P. C. Deshmukh, T. Banerjee, K. P. Sunanda, and H. R. Varma, Radiat. Phys. Chem. **75**, 2211 (2006).